



Effect of bismuth ion substitution on structural properties of zinc ferrite nanoparticles

Naraavula Suresh Kumar¹, Katrapally Vijaya Kumar^{2,*}

¹Mallareddy Institute of Engineering & Technology, Maisammaguda, Secunderabad-500014, TS, India

²Department of Physics, JNTUH College of Engineering Jagtial, Nachupally (Kondagattu), Karimnagar (Dist.) 505501, TS, India

Received 24 April 2016; Received in revised form 27 June 2016; Accepted 30 June 2016

Abstract

Bismuth doped nano zinc ferrite particles having the general formula $ZnFe_{2-x}Bi_xO_4$ ($x = 0.00, 0.05, 0.10, 0.15, 0.20$ and 0.25) were synthesized by sol-gel combustion method. The effect of bismuth doping on structural properties were investigated. The X-ray diffraction (XRD) spectra confirm the single phase cubic spinel structure. The average crystallite sizes of all the samples were determined by Debye-Scherrer equation and are in the range 16–20 nm. The lattice parameter increases with the increase of bismuth ion concentration. This is due to the larger ionic radius of Bi^{3+} ions substituting smaller Fe^{3+} ions at octahedral sites (B-sites). The surface morphology of all compounds was studied by scanning electron microscope (SEM). The microstructure analysis and the particle size were examined by transmission electron microscope (TEM). The compositional stoichiometry of these samples was verified by energy dispersive spectroscopy (EDS) analysis.

Keywords: Zn-Bi ferrites, nanopowder, sol-gel combustion method, XRD, SEM, TEM, EDS

I. Introduction

Nanosized ferrites are magnetic ceramics of great importance in microwave and electromagnetic applications [1,2]. The ferrite materials exhibit great physical and chemical properties specifically in the nano-range [3,4]. The normal spinel structure of any ferrite material has general formula AB_2O_4 , where divalent metal cations are located on the tetrahedral A-sites, whereas the octahedral B-sites are preferably occupied with trivalent metal cations [5,6]. $ZnFe_2O_4$ has a normal spinel structure with Zn^{2+} metal cation belonging to tetrahedral sites (A-site) and Fe^{3+} metal cation holding octahedral sites (B-site) [7,8]. However, in inverse spinel structure the divalent metal cations occupy octahedral sites and trivalent metal cations occupy tetrahedral and octahedral sites equally. $CoFe_2O_4$ is the best example for inverse spinel structure with Co^{2+} ions at octahedral sites and Fe^{3+} ions equally occupying both tetrahedral and octahedral sites [9]. The structural properties and physicochemical properties of ferrites can be modified by doping with different divalent and trivalent metal ions

at tetrahedral and octahedral positions, like Mg, Ni, Co, Ba, Sr, Li, Ti, Ca, Nb, Cd, Bi, Mn, Zn etc. Out of different elements present in the periodic table it is assumed that bismuth is one of potential dopant elements to alter properties due to its high electrical resistivity with low magnetic and dielectric losses [10–13]. Hence bismuth doped ferrites (BFO) are widely used in magnetic recording, high density data storage devices and microwave device applications. The present work is focused on the effect of bismuth substitution on structural properties of zinc ferrite nanoparticles.

II. Experimental

A series of bismuth doped zinc ferrite nanoparticles of the chemical formula $ZnFe_{2-x}Bi_xO_4$ ($x = 0.00, 0.05, 0.10, 0.15, 0.20$ and 0.25) was synthesized by sol-gel combustion method. Probably this is the most effective method to fabricate highly pure nanocrystalline powder samples with mostly uniform grain sizes [14,15]. The stoichiometric amounts of the metal nitrates taken in a beaker were completely dissolved in double distilled water with constant stirring using a magnetic stirrer. The citric acid in the molar ratio 1:3 with the metal nitrates was added. Under the constant stirring an appro-

*Corresponding author: tel: +98 917 1197591, fax: +98 3613 415628, e-mail: kvkphd@gmail.com

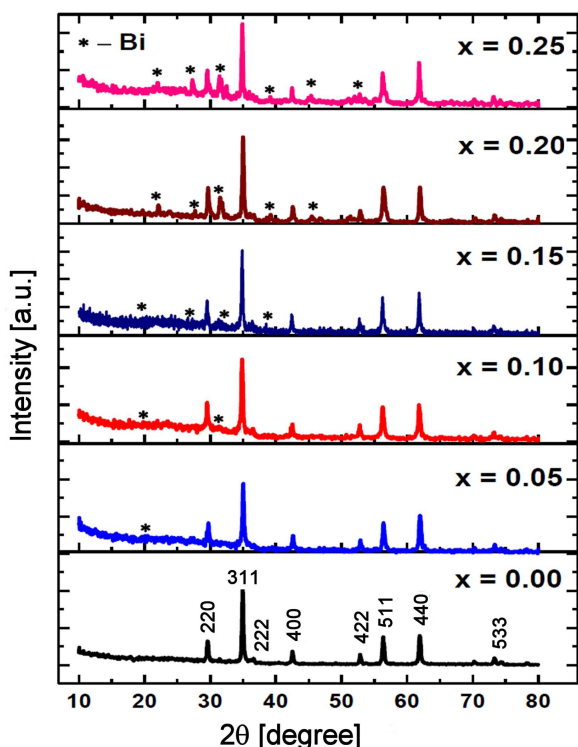


Figure 1. XRD patterns of $ZnFe_{2-x}Bi_xO_4$ ($0.00 \leq x \leq 0.25$) powders calcined at $600^\circ C$

appropriate amount of ammonia solution was added drop wise until a homogeneous solution was obtained and pH~7 had been reached. The mixed solution was then evaporated at constant temperature for 2–3 h until the solution turned into a dark viscous gel. The prepared gels were further heated to 120–150 °C and a dark ash powder was yielded. Then the powders were cooled to room temperature and grained in an agate mortar to get fine crystalline powders. Finally, the prepared powder samples were calcined at 600 °C for 5 h in air and characterized by XRD, SEM, TEM and EDS for structural properties.

The phase identification and lattice parameters of the

prepared samples were carried out by X-ray diffractometer (PN1710 Phillips) using $CuK\alpha$ ($\lambda = 1.54 \text{ \AA}$) radiation. The surface morphology of the samples was observed by the use of scanning electron microscope (SEM, Oxford Instruments, EVO 18 SEM-ZEISS) and the microstructure analysis was observed by transmission electron microscope (TEM, Model KT150, Kerry Ultrasonic Ltd.). The composition analysis was done with energy dispersive spectrometer (EDS, Oxford Instruments, EVO 18 SEM-ZEISS).

III. Results and discussion

3.1. X-ray diffraction analysis

Figure 1 shows the X-ray diffraction (XRD) patterns of $ZnFe_{2-x}Bi_xO_4$ ($0.00 \leq x \leq 0.25$) ferrite nanoparticles. The XRD results confirm the single phase spinel structure of the pure $ZnFe_2O_4$ [16]. The XRD also confirms that the addition of bismuth in small quantity does not alter the spinel structure of ferrite system [17], but the additional peaks in the samples containing bismuth indicate the existence of a secondary phase (Fig. 1). The crystallite size (D) of all compounds was determined from broadening of the XRD peak 311 using Debye-Scherrer formula following (Eq. 1):

$$D = \frac{0.9\lambda}{\beta \cdot \cos \theta} \quad (1)$$

where, D is the average crystallite size of the phase under investigation, λ is wavelength of X-ray beam used, β is full width at half maxima (FWHM) in radians and θ is Bragg's angle. It is observed from Table 1 that crystallite size (D) increases from 16 nm to 20 nm and lattice constant (a) increases from 8.3743 to 8.4207 Å with the increase of Bi^{3+} ion concentration as shown in Fig. 2a. This may be attributed to the partial replacement of smaller Fe^{3+} (0.64 Å) with larger Bi^{3+} (1.31 Å) ions at octahedral sites. Similar behaviour was observed by Nasr Isfahani [18] in bismuth doped nickel ferrites. The

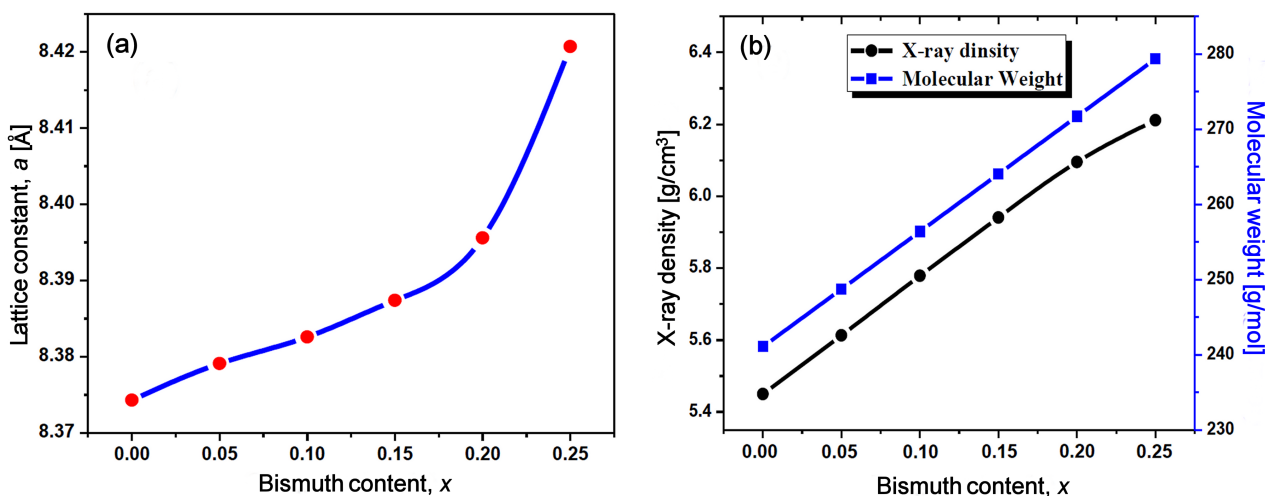


Figure 2. Variation of lattice constant (a) and X-ray density and molecular weight (b) of $ZnFe_{2-x}Bi_xO_4$ ($0.00 \leq x \leq 0.25$) powders calcined at $600^\circ C$ with bismuth content

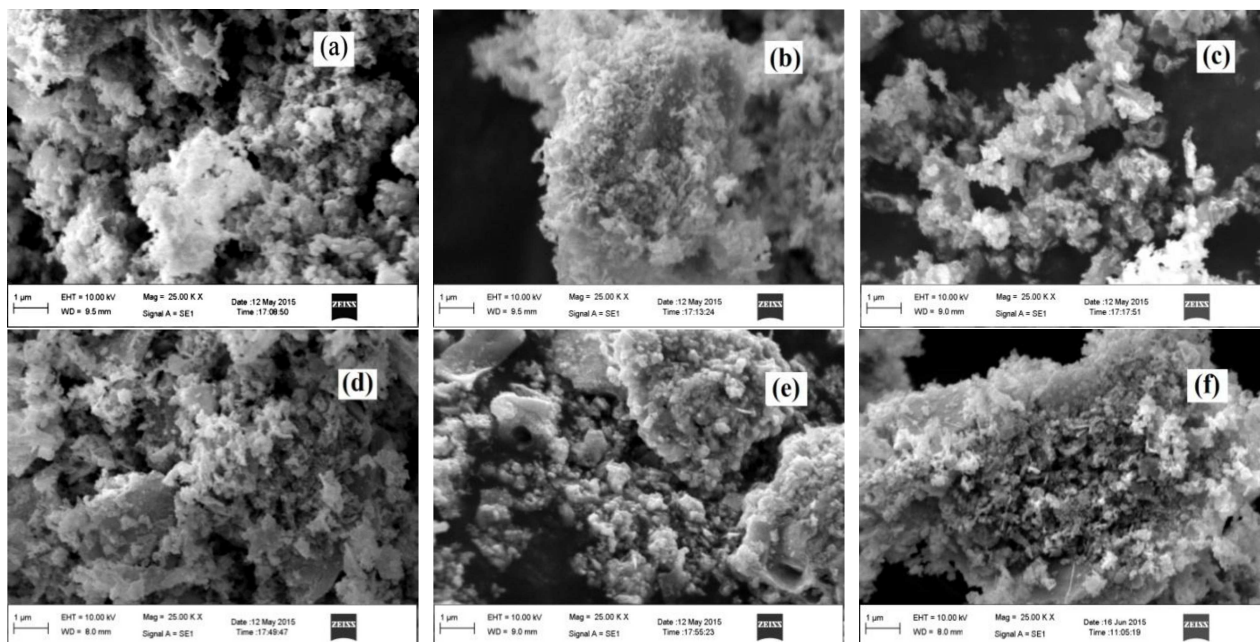


Figure 3. SEM images of ZnFe_{2-x}Bi_xO₄ calcined at 600 °C: a) $x = 0$, b) $x = 0.05$, c) $x = 0.1$, d) $x = 0.15$, e) $x = 0.2$ and f) $x = 0.25$

Table 1. Crystallite size (D), lattice constant (a), X-ray density (ρ_{XRD}), bulk density (ρ_B), molecular weight (M), inter planar distance (d) and porosity (P) of ZnFe_{2-x}Bi_xO₄ ($0.00 \leq x \leq 0.25$) calcined at 600 °C

Bi content	D [Å]	a [Å]	ρ_{XRD} [g/cm ³]	ρ_B [g/cm ³]	M [g/mol]	d [Å]	P [%]
0.00	16.8667	8.3743	5.4497	4.801	241.08	2.5249	11.91
0.05	17.5476	8.3791	5.6132	5.088	248.74	2.5264	9.35
0.10	17.6777	8.3826	5.7788	5.027	256.40	2.5274	13.0
0.15	19.2286	8.3874	5.9408	4.974	264.04	2.5289	16.27
0.20	20.2931	8.3956	6.0953	5.458	271.70	2.5313	10.45
0.25	20.6422	8.4207	6.2112	5.368	279.36	2.5389	13.57

lattice constant (a) of all nanopowders was determined by the following equation:

$$a = d\sqrt{h^2 + k^2 + l^2} \tag{2}$$

where h , k and l are the Miller indices of the crystal plane. The X-ray density (ρ_{XRD}), bulk density (ρ_B) and porosity (P) are shown in Table 1. The X-ray density (ρ_{XRD}) was calculated using the following equation:

$$\rho_{XRD} = \frac{8M}{N \cdot a^3} \tag{3}$$

where, M is molecular weight of the sample, N is Avogadro’s number. The X-ray density (ρ_{XRD}) of any ferrite system was affected by the lattice constant (a) and the molecular weight (M) of ferrite compound [19]. From Fig. 2b it was observed that the X-ray density gradually increases with the increase of bismuth ion concentration. This may be ascribed to the higher atomic weight of bismuth ions (208.98 g/mol) compared to the atomic weight of ferric ions (55.85 g/mol).

3.2. SEM – TEM analysis

Figure 3 shows the microscopic SEM images of the prepared ZnFe_{2-x}Bi_xO₄ ($0.00 \leq x \leq 0.25$) powders.

From the SEM images it is clear that the particles are distributed homogeneously with low degree of agglomeration. It is evident that the primary particles are within nanoscale region.

The surface morphology and microstructure of the ZnFe₂O₄, ZnBi_{0.1}Fe_{1.9}O₄ and ZnBi_{0.2}Fe_{1.8}O₄ nanopowders are shown on TEM images (Fig. 4). It can be observed that the particles were spherical in shape forming loose aggregates. However, some moderately agglomerated particles as well as separated particles are also present in these images. The corresponding selective area electron diffraction (SAED) of these samples indicates that the bismuth doped Zn-ferrite nanoparticles have well crystalline nature with the inter-planar spacing in good agreement with the XRD result.

3.3. EDS analysis

Figure 5 shows EDS spectra of the prepared ZnFe_{2-x}Bi_xO₄ ($0.00 \leq x \leq 0.25$) nanoparticles calcined at 600 °C. The relative elemental composition (in wt.% and at.%) of all powders are shown in Table 2. EDS data reveal the presence of Zn²⁺, Fe³⁺, Bi³⁺ and O⁴⁻ ions in appropriate proportions as desired in considered compounds with an error of up to 0.2%.

Table 2. Relative elemental composition of $\text{ZnFe}_{2-x}\text{Bi}_x\text{O}_4$ ($0.00 \leq x \leq 0.25$) powders calcined at 600°C

Sample composition, x	O		Zn		Bi		Fe	
	[wt.%]	[at.%]	[wt.%]	[at.%]	[wt.%]	[at.%]	[wt.%]	[at.%]
0.00	27.11	57.86	27.20	14.21	–	–	45.69	27.94
0.05	24.69	55.73	27.08	16.33	4.21	1.73	44.04	26.31
0.10	24.31	56.38	25.76	14.23	8.73	1.55	41.98	27.89
0.15	23.47	56.19	25.41	14.88	12.20	2.24	38.92	26.69
0.20	23.14	57.75	24.88	14.18	16.87	2.99	35.14	24.80
0.25	23.05	56.73	23.24	14.02	19.67	3.43	33.97	23.95

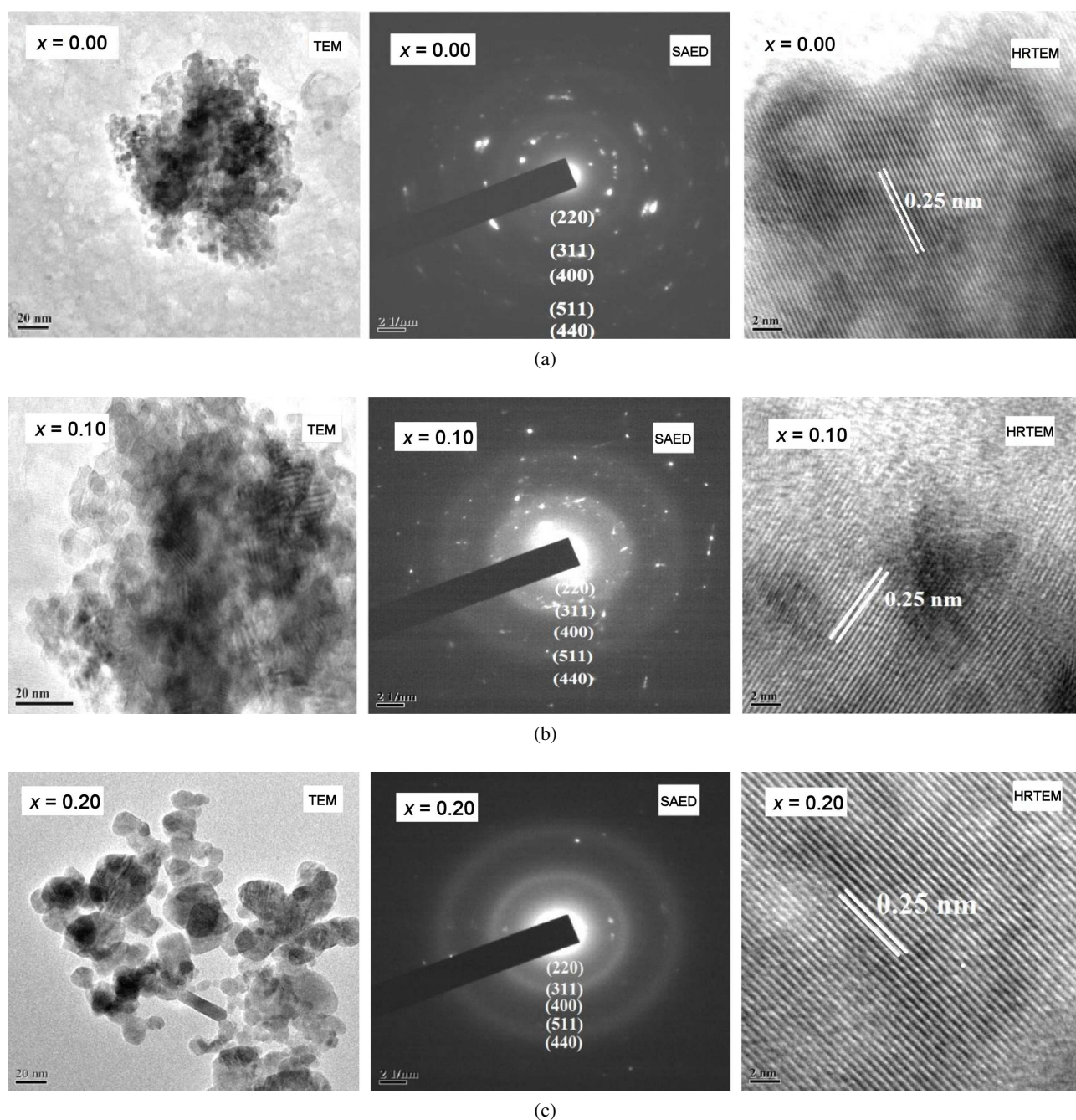


Figure 4. TEM, SAED and HRTEM images of: a) ZnFe_2O_4 , b) $\text{ZnBi}_{0.1}\text{Fe}_{1.9}\text{O}_4$ and c) $\text{ZnBi}_{0.2}\text{Fe}_{1.8}\text{O}_4$ powders calcined at 600°C

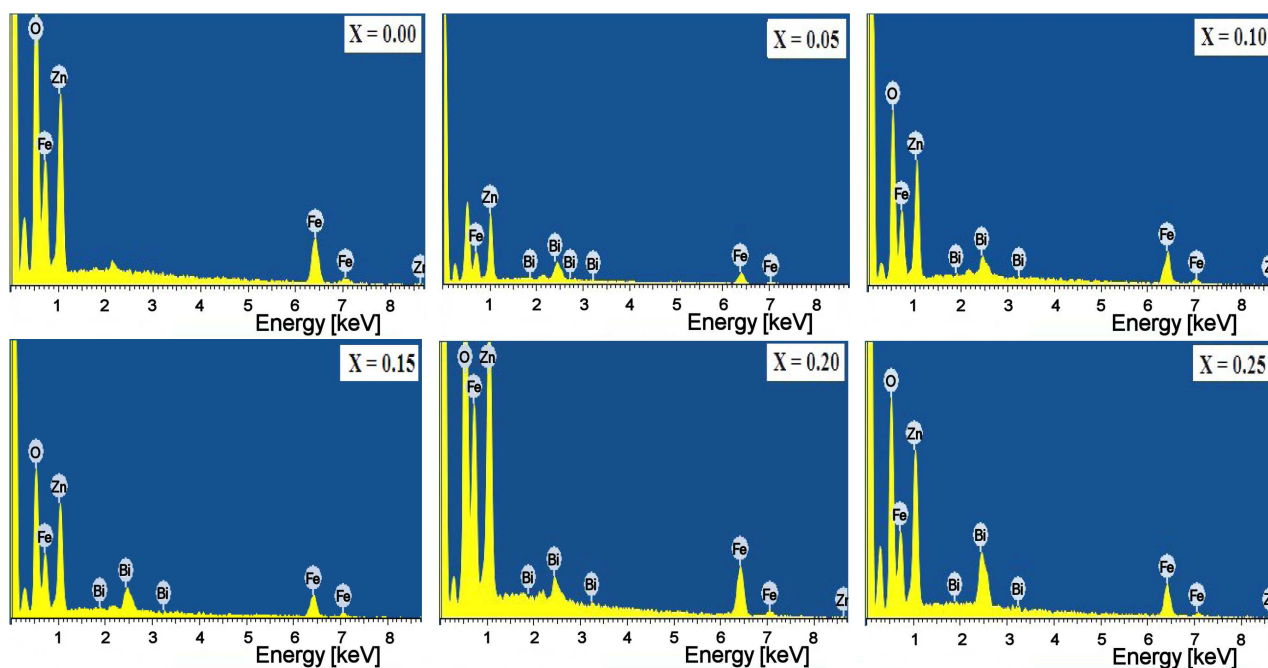


Figure 5. EDS spectra of $\text{ZnFe}_{2-x}\text{Bi}_x\text{O}_4$ ($0.00 \leq x \leq 0.25$) powders calcined at 600°C

IV. Conclusions

A series of bismuth doped zinc ferrite nanoparticles was successfully synthesized by sol-gel combustion method. All prepared samples were calcined at 600°C for 5 h in air. The X-ray diffraction patterns confirmed the formation of single phase spinel structure in the pure ZnFe_2O_4 and the existence of a secondary phase in the samples containing bismuth. The crystallite size of the prepared samples was found to be in the range 16–20 nm. The lattice parameter is found to increase with the increase of bismuth ion concentration. This is due to the larger ionic radius of Bi^{3+} replacing smaller Fe^{3+} ions at octahedral sites (B-sites). The surface morphology confirmed uniform structure of all nanopowders and the crystallite size being lower than 20 nm. Finally, the patterns of elemental analysis (EDS) show the presence of stoichiometric elements in required proportions in all compounds.

Acknowledgments: The author NSK is thankful to Dr. K.E. Balachandrudu, Principal, MRIET, Secunderabad for providing the necessary facilities to bring out this research work. Dr. KVK is grateful to Prof. N.V. Ramana, Principal, JNTUH College of Engineering Jagtial, Nachupally (Kondagattu), Karimnagar-Dist for his encouragement.

References

1. A.M. Abo El Ata, S.M. Attia, T.M. Meaz, "AC conductivity and dielectric behavior of $\text{CoAl}_x\text{Fe}_{2-x}\text{O}_4$ ", *Solid State Sci.*, **6** (2004) 61–69.
2. W.A. Bayoumy, M.A. Gabal, "Synthesis characterization and magnetic properties of Cr-substituted NiCuZn nanocrystalline ferrite", *J. Alloys Compd.*, **506** (2010) 205–209.
3. V. Pallai, D.O. Shah, "Synthesis of high-coercivity cobalt ferrite particles using water-in-oil microemulsions", *J. Magn. Magn. Mater.*, **163** (1996) 243–248.
4. R. Skomski, "Nanomagnetics", *J. Phys.: Condens. Matter*, **15** (2003) R841–R896.
5. C. Venkataraju, G. Sathish Kumar, K. Sivakumar, "Effect of Cd on the structural, magnetic and electrical properties of nanostructured Mn-Zn ferrite", *J. Magn. Magn. Mater.*, **323** (2011) 1817–1822.
6. Q. Fang, H. Cheng, K. Huang, J. Wang, R. Li, "Doping effect on crystal structure and magnetic properties of chromium-substituted strontium hexaferrite nanoparticles", *J. Magn. Magn. Mater.*, **294** (2005) 281–286.
7. F.J. Burghart, W. Potzel, G.M. Kalvius, E. Schreier, G. Grosse, D.R. Noakes, W. Schafer, W. Kockelmann, S.J. Campbell, W.A. Kaczmarek, A. Martin, M.K. Krause "Magnetism of crystalline and nanostructured ZnFe_2O_4 ", *Physica B*, **289** (2000) 286–290.
8. L.D. Tung, V. Kolesnichenko, G. Caruntu, Y. Remond, V.O. Golub, C.J. O'Connor, L. Spinu, "Annealing effects on the magnetic properties of nanocrystalline zinc ferrite", *Physica B*, **319** (2000) 116–121.
9. D.S. Mathew, R.S. Juang, "An overview of structure and magnetism of spinel ferrite nanoparticles and their synthesis in microemulsions", *J. Chem. Eng.*, **129** [1-3] (2007) 51–65.
10. M. Pardavi-Horvath, "Microwave applications of soft ferrites", *J. Magn. Magn. Mater.*, **215-216** (2000) 171–183.
11. N. Gupta, M.C. Dimri, S.C. Kashyap, D.C. Dube, "Processing and properties of cobalt substituted lithium ferrite in the GHz frequency range", *Ceram.*

- Int.*, **31** (2005) 171–176.
12. G. Bate, “Synthesis and structural properties of bismuth doped cobalt nanoferrites prepared by sol-gel combustion method”, pp. 703 in *Magnetic Oxides, Part 2*, Ed. D.J. Craik, Wiley Interscience, New York, USA, 1975.
 13. M.P. Sharrock, “Particulate magnetic recording media: A review”, *IEEE Trans. Magn.*, **25** (1989) 4374–4389.
 14. N. Suresh Kumar, K. Vijaya Kumar, “Synthesis and structural properties of bismuth doped cobalt nanoferrites prepared by sol-gel combustion method”, *World J. Nano Sci. Eng.*, **5** (2015) 140–151.
 15. P.P. Hankare, V.T. Vader, U.B. Sankpal, L.V. Gavali, R. Sasikala, I.S. Mulla, “Effect of sintering temperature and thermoelectric power studies of the system $\text{MgFe}_{2-x}\text{Cr}_x\text{O}_4$ ”, *Solid State Sci.*, **11** (2009) 2075–2079.
 16. A. Hassadee, T. Jutarosaga, W. Onreabroy, “Effect of zinc substitution on structural and magnetic properties of cobalt ferrite”, *Procedia Eng.*, **32** (2012) 597–602.
 17. F. Bensebaa, F. Zavaliche, P. L’Ecuyer, “Microwave synthesis and characterization of Co-ferrite nanoparticles”, *J. Colloid Interface Sci.*, **277** (2004) 104–110.
 18. M.J. Nasr Isfahani, M. Jafri Fesharaki, “Magnetic behavior of nickel-bismuth ferrite synthesized by a combined sol-gel/thermal method”, *Ceram. Int.*, **39** (2013) 1163–1167.
 19. A. Goldman, *Modern Ferrite Technology*, Van Nostrand Reinhold, New York, USA, 1990.